remote sensing

MDPI

Technical Note

Analysis of Cassini Altimetric Crossovers on Titan

Daniele Durante [1,*], Marco Mastrogiuseppe [1,2], Elisa Carli [1], Valerio Poggiali [3], Andrea Di Ruscio [1,4], Virginia Notaro [1,4] and Luciano Iess [1]

[1] Department of Mechanical and Aerospace Engineering, Sapienza University of Rome, 00184 Rome, Italy; marco.mastrogiuseppe@uniroma1.it (M.M.); elisa.carli@univ-tlse3.fr (E.C.); andrea.diruscio@thalesaleniaspace.com (A.D.R.); virginia.notaro@thalesaleniaspace.com (V.N.); luciano.iess@uniroma1.it (L.I.)
[2] Department of Human Sciences, Link Campus University, 00165 Rome, Italy
[3] Cornell Center for Astrophysics and Planetary Science, Cornell University, Ithaca, NY 14850, USA; vpoggiali@astro.cornell.edu
[4] Thales Alenia Space, 00131 Rome, Italy
* Correspondence: daniele.durante@uniroma1.it

Abstract: The Cassini spacecraft performed several flybys of Saturn's largest moon, Titan, collecting valuable data. During several passes, altimetric data were acquired. Here, we focus on altimetric measurements collected by Cassini's radar when flying over the same region at different epochs in order to correlate such measurements (crossovers) and investigate differences in altimetry. In our study, we assess altimetric errors associated with three distinct methods for extracting topography from Cassini's radar data: the maximum likelihood estimator (MLE), the threshold method, and the first moment technique. Focusing on crossover events, during which Cassini revisited specific areas of Titan's surface, we conduct a detailed examination of the consistency and accuracy of these three topography extraction methods. The proposed analysis involves closely examining altimetric data collected at different epochs over identical geographical regions, allowing us to investigate potential errors due to the variations in off-nadir angle, relative impact, uncertainties, and systematic errors inherent in the application of these methodologies. Our findings reveal that the correction applied for the off-nadir angle to the threshold and first moment methods significantly reduces the dispersion in the delta difference at the crossover, resulting in a dispersion of the order of 60 m, even lower than what is achieved with the MLE (~70 m). Additionally, an effort is made to assess the potential of Cassini for estimating the tidal signal on Titan. Considering the altimetric errors identified in our study and the relatively low number of crossovers performed by Cassini, our assessment indicates that it is not feasible to accurately measure the tidal signal on Titan using the currently available standard altimetry data from Cassini. Our assessment regarding the accuracy of the Cassini altimeter provides valuable insights for future planetary exploration endeavors. Our study advances the understanding of Titan's complex landscape and contributes to refining topographical models derived from Cassini's altimetry observations. These insights not only enhance our knowledge of Saturn's largest moon but also open prospects for Titan surface and interior exploration using radar systems.

Keywords: Cassini; Titan; radar altimetry; crossover; orbit determination; radio science

Citation: Durante, D.; Mastrogiuseppe, M.; Carli, E.; Poggiali, V.; Di Ruscio, A.; Notaro, V.; Iess, L. Analysis of Cassini Altimetric Crossovers on Titan. *Remote Sens.* **2024**, *16*, 2209. https://doi.org/10.3390/rs16122209

Academic Editor: Chein-I Chang

Received: 12 April 2024
Revised: 10 June 2024
Accepted: 12 June 2024
Published: 18 June 2024

1. Introduction

The NASA/ESA/ASI Cassini–Huygens mission spanned nearly 20 years in deep space, with 13 years dedicated to exploring the Saturnian system and the planet Saturn, including its rings and natural satellites. Throughout its journey within the system, the Cassini spacecraft performed multiple flybys of Saturn's largest moon, Titan, collecting valuable scientific data. During several passes, altimetric data were acquired with the Cassini RADAR instrument [1]. Hidden by an optically thick nitrogen atmosphere, the RADAR

instrument successfully revealed Titan's surface, characterized by a rich and diverse set of morphologies [2]. These included dune fields at equatorial latitudes [3–5], mountains [6], and hydrocarbon lakes and seas at the poles [7,8], which sometimes appeared desiccated as empty basins [9,10]. In the polar regions, Titan's methane-based hydrologic system [11,12] produced precipitations that fed channels and canyons [13], where liquids flowed into the seas, creating series of familiar coastal sedimentary deposits [14].

The striking Ku-band microwave transparency of liquid hydrocarbons was exploited during several altimetric and radiometric observations to provide some insight into seas' depth and composition [15–20].

Here, we focus on altimetric measurements by analyzing those collected by Cassini when flying in the same region of the moon but at a different epoch (therefore, a different Titan flyby) in order to correlate such measurements (crossover) and investigate differences in altimetry.

Figure 1 shows altimetry tracks where crossovers can be identified (see Section 4), and Table 1 provides a summary of information about these flybys. Note that these are a subset of Cassini altimetry tracks over Titan. We found a total of 11 pairs of tracks where crossover points can be identified. Our analysis of altimetric crossovers aims to characterize the performance of Cassini's radar in altimetry mode and investigate potential physical displacement of the surface due to tides. Cassini's determination of the time varying component of Titan's gravity field [21,22], forced by Saturn's tidal perturbation on Titan's eccentric orbit, proved to be a valuable measurement to infer the presence of an internal ocean. Indeed, Titan's gravitational shape is largely deformed by an amount so large that only an elastic interior can provide. The latest determination of the Love number k_2 [22] is compatible with that of a water mantle (consisting of various solid and liquid phases) that is substantially more dense than pure water. However, the large variability of Titan's gravitational shape due to eccentricity tides does not guarantee a large variability of Titan's shape (i.e., if the crust is rigid).

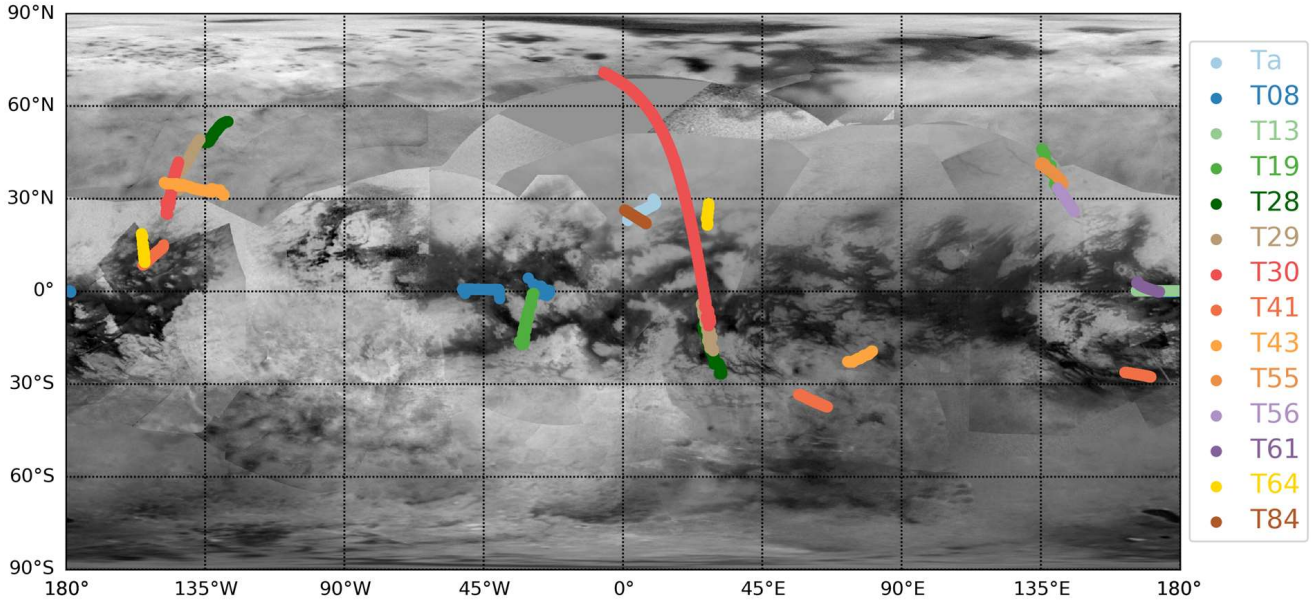

Figure 1. Altimetry tracks of Cassini over Titan's surface where a crossover can be identified. The background image is a global mosaic from Cassini ISS instrument (from NASA PSD).

Table 1. Summary of Cassini altimetry tracks over Titan used in the analysis.

Flyby	Date (UTC)	Minimum Altitude	Mean Anomaly, M
Ta	26 October 2004 15:31:27	1174 km	−59°
T08	28 October 2005 04:15:24	1353 km	−66°
T13	30 April 2006 20:58:14	1856 km	145°
T19	9 October 2006 17:30:07	980 km	−163°
T28	10 April 2007 22:58:00	991 km	14°
T29	26 April 2007 21:32:58	981 km	14°
T30	12 May 2007 20:09:58	959 km	14°
T41	22 February 2008 17:32:07	1000 km	−12°
T43	12 May 2008 10:01:58	1001 km	−13°
T55	21 May 2009 21:26:30	965 km	161°
T56	6 June 2009 19:59:36	965 km	161°
T61	25 August 2009 12:51:37	970 km	160°
T64	27 December 2009 00:16:59	955 km	90°
T84	6 June 2012 00:07:21	959 km	67°

2. Titan Shape

Being tidally locked, along its revolution around Saturn every almost 16 days, Titan experiences a strong tidal perturbation from the planet, which stretches the moon, producing a triaxial ellipsoidal shape, with the long axis pointed toward the planet. Titan's ellipsoidal shape at colatitude θ and longitude φ is given by:

$$R(\theta, \varphi) = R_T[1 + H_{20}P_{20}(\cos\theta) + H_{22}P_{22}(\cos\theta)\cos(2\varphi)]$$

where R_T is Titan's mean radius (2575 km), $P_{20}(\cos\theta)$ and $P_{22}(\cos\theta)$ are associated Legendre polynomials of degree 2 and order, respectively, 0 and 2, while H_{20} and H_{22} are spherical harmonic coefficients. Assuming only the effect of tides and rotation, these coefficients are given by:

$$\begin{cases} H_{20} = -(\frac{q_t}{6} + \frac{q_r}{3})h_2^f = -\frac{5}{6}q_r\, h_2^f \\ H_{22} = \frac{1}{12}q_t\, h_2^f = \frac{1}{4}q_r\, h_2^f \end{cases}$$

where h_2^f is the fluid Love number of degree 2 associated with the radial displacement of the solid tide, while q_t and q_r are, respectively, the tidal and rotational parameters, given by:

$$q_t = 3q_r = 3\frac{M_s}{M_T}\left(\frac{R_T}{a}\right)^3$$

where M_s is Saturn's Mass, M_T is Titan's mass, and a is the semi-major axis of Titan's orbit around Saturn. For a hydrostatic body, the ratio H_{20}/H_{22} is equal to $-10/3$. Different shape models obtained with Cassini's imaging and radar systems determined that Titan's shape slightly deviates from the hydrostatic expectation [23,24].

Eccentricity Tides

Since Titan's orbit has a small eccentricity (about 0.0288), its distance from Saturn slightly changes, thus letting Titan experience a time variable tidal perturbation. The time variable tidal attraction causes a time variable deformation of its gravitational shape, which is largely affected due to the presence of an internal ocean. This phenomenon is controlled by the tidal Love number k_2, which has been determined very accurately through analysis of Cassini gravity data (k_2 = 0.616 ± 0.067 [22]). At the same time, the physical surface of

the moon may also be displaced (i.e., solid tide). This is controlled by the Love number h_2 (at tidal frequency), which governs the amplitude of the response as Titan moves along its orbit about Saturn and depends on the interior structure properties. At first order in inclination and eccentricity, Titan's shape harmonic coefficients are time variable:

$$\begin{cases} \Delta H_{20} = \frac{1}{2} q_t \, h_2 \, e \cos M \\ \Delta H_{22} = \frac{1}{4} q_t \, h_2 \, e \cos M \end{cases}$$

That is, the solid tide signal is controlled over the orbit by the mean anomaly, M. Assuming a Love number h_2 = 2.5, the maximum tidal signal at the sub-Saturnian point is about 22 m when Titan is at the pericenter or apocenter (with opposite signs). Several theoretical studies have evaluated the effects of tides on Titan's surface, both solid and liquid [25], and the possibility of detecting them using radar techniques [26]. In our work, we make use of altimetric data to investigate the possibility of estimating Titan's tidal signal.

Since Cassini's radar in altimetry mode is always looking towards the center of the moon (neglecting off-nadir angles, which are generally small), the correction of altimetric measurements due to the tidal signal is, to first order:

$$\Delta r = R_T \left[\Delta H_{20} P_{20}(\cos\theta) + \Delta H_{22} P_{22}(\cos\theta) \cos(2\varphi) \right]$$

3. Radar Altimetry

The Cassini radar was designed as a versatile instrument capable of operating in multiple modes, including synthetic aperture radar (SAR) for surface imaging, radar altimeter for topography measurements, scatterometer for surface composition, and, in passive mode, as a radiometer for brightness temperature [27]. During each Titan flyby, the instrument modes were sequentially activated, starting from an altitude of 100,000 km and descending to 1000 km at the closest approach. The antenna was strategically positioned to conduct the targeted measurements. Detailed descriptions of sequence planning and instrument performance can be found in [28]. Through 53 dedicated flybys for radar observations, Cassini managed to map approximately 50% of Titan's surface with a resolution of less than 1 km in SAR mode and acquired 40 topographic profiles in altimetry mode [1].

During the Cassini mission, the altimetry dataset played an important role in unraveling Titan's diverse landscape. Altimetric data were systematically collected by pointing the antenna toward Titan's center of mass, allowing for the transmission and reception of 15 pulses during each data acquisition. These observations were performed using bursts of frequency-modulated signals with a bandwidth of 4.25 MHz, achieving a nominal radar resolution δ of 35 m in a vacuum (see [1], for more details). This capability, combined with Cassini spacecraft geometry, furnished a horizontal resolution ranging from 55 to 6 km, offering detailed insights into the moon's varied topography.

Altitude variations, spanning from 1000 to 9000 km, significantly influenced the achieved resolution, underscoring the dataset's adaptability to different altitudinal contexts. The spacecraft's precision was evident in maintaining off-nadir angles typically less than a fraction of the antenna beamwidth (0.35°), ensuring the accuracy of the altimetric measurements.

The radar footprint on the surface depended on the operative conditions, which were determined by the spacecraft altitude. In a beam-limited configuration, Cassini's radar aperture (θ = 0.35 degrees) determined the geometrical footprint. The radius is given by:

$$r_b = \frac{H \, \theta}{\sqrt{2.8}}$$

where H is the altitude over Titan's surface. At an altitude of 4000 km, the footprint radius was about 15 km. At a higher altitude, Cassini radar operated in a pulse-limited configuration, where the radar resolution determined the footprint (i.e., the area that can

be resolved). In this scenario, the radius of the footprint, r_p, was smaller than that of the geometrical footprint. It can be computed by:

$$r_p = \sqrt{2H\delta}$$

The transition between the two modes occurred at an altitude of about 7500 km [29]. At that altitude, the beam-limited footprint radius was 27 km, whereas the pulse-limited radius was only about 23 km at the surface.

Altimetry Datasets

The altimetric data recorded by the Cassini RADAR instrument underwent various processing methods, resulting in distinct datasets that captured different aspects of Titan's surface. Thus, different datasets exist:

- Maximum likelihood estimator (MLE). This dataset was developed based on a statistical model [29,30], particularly the Brown model initially utilized to measure sea roughness. MLE optimally estimates parameters by maximizing the likelihood function, showcasing its asymptotically unbiased and efficient characteristics;
- Threshold. This dataset was acquired through a tracking algorithm employed as a thresholding mechanism [31]. This method is particularly sensitive to the higher portions of the surface, capturing portions of the echoes above a specified threshold. It serves as an effective means of tracking prominent features on Titan's surface;
- First moment. This dataset was generated by computing the first moment from the returned waveform. This involves estimating the centroid of the power distribution, providing a mean value for the surface. This method, rooted in centroid estimation of the pulse width, contributes valuable insights into surface characteristics.

Additionally, for the last two datasets, off-nadir angle corrections can be applied using specific models. Note that the model used in the MLE technique already accounts for off-nadir angles. These datasets are available on the NASA Planetary Data System (PDS) system (see the Data Availability Section). The left panel of Figure 2 shows the different altimetry profiles obtained for a given pass.

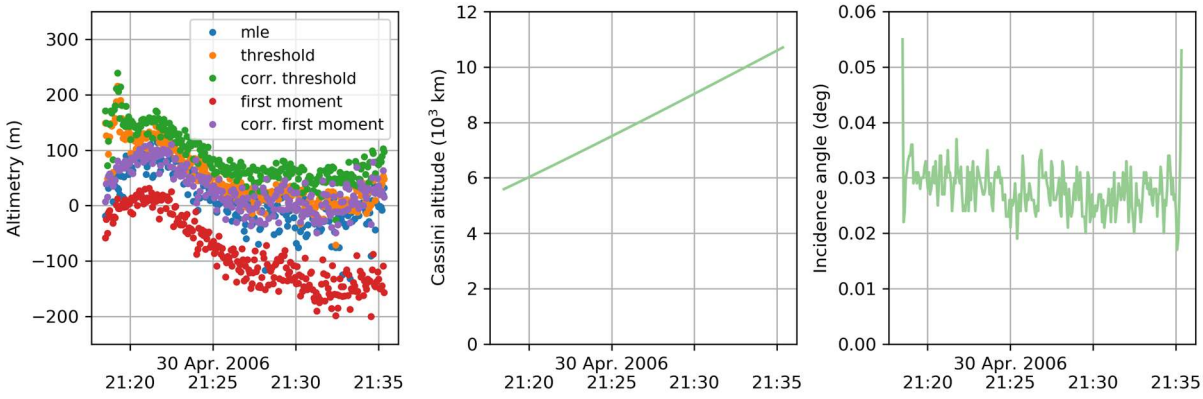

Figure 2. Left panel: altimetry profile obtained with different algorithms; **middle panel**: Cassini altitude over Titan (range to ellipsoid)'s profile; **right panel**: off-nadir radar angle, for a selected pass (T13).

Complementing traditional altimetry processing, an advanced processing chain was applied to raw altimetry Cassini data (LBDR, long burst data record). This involved coherent Doppler processing, which substantially improved along-track resolution and signal-to-noise ratio (SNR) compared with existing altimeter burst data record (ABDR) data [32]. This advanced processing elevated the quality of the altimetry dataset, not only providing a comprehensive view of Titan's global topography but also offering detailed insights into features such as dunes and bathymetry of seas and lakes. This dataset can, in

principle, improve the quality of the Cassini altimetry dataset, but, for now, we prefer to focus our work on the standard dataset currently available on the NASA PDS node and leave the analysis of the delay-Doppler altimetry data for future work.

Due to the large superimposition between adjacent footprints and in order to reduce the altimetry noise, we averaged the data points to obtain a smoother profile. In our analysis, we used a Savitzky–Golay filter with a linear fit over a window length, which was selected for each pass in order to have, on average, an overlap between adjacent footprints of about 50% on the along-track direction. Such a choice resulted in a number of points ranging from 5 to 15, according to altitude and tangential velocity of each altimetry pass. This allowed us to follow as close as possible the underlaying topography, while removing high-frequency noise. The same procedure has been proven successful in previous analysis, e.g., in Titan dune height retrieval [33].

4. Crossover Identification

A crossover is typically defined when two tracks intersect; in this case, the crossover is the intersection point. In such a configuration, we can suppose to observe the same topography. If the tidal signal is the same (i.e., the difference in the mean anomaly is equal to zero, or the mean anomalies have opposite signs), then we can directly measure the altimetry errors from the difference of the topography retrieved from the two observations. We extend the crossover definition to also account for configurations in which the two ground tracks do not intersect but the radar footprints overlap. We can expect a large degree of correlation between the recovered topography if the two footprints largely overlap. Therefore, for a given pair of tracks, we look for the footprint overlap. When more than one point can be identified, we select the crossover as the pair of points at which the distance between the tracks over Titan's surface is minimum.

A summary of the flyby pairs found are reported in Table 2, for a total of 11 crossover (or footprint overlaps) identified by an uppercase letter. The altimetry tracks and corresponding radar footprints are reported in Figure 3. Note that six crossovers have a null or very small difference in the mean anomaly, meaning that the solid tidal signal is expected to be the same. These observations are used to test the accuracy of the crossover points, without the effect of solid tides.

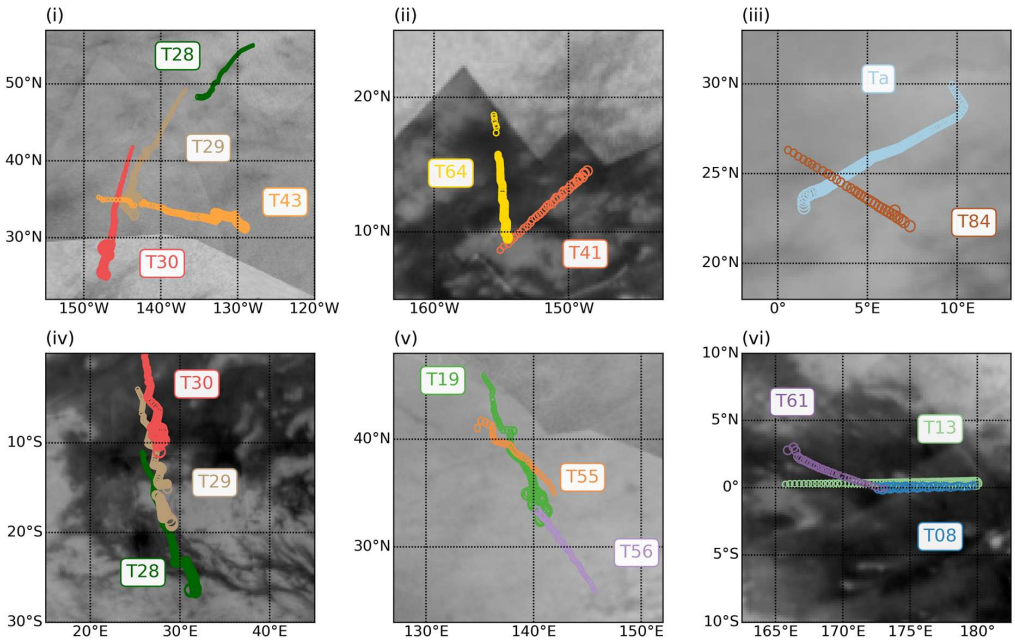

Figure 3. Zoom on altimetry tracks of Cassini over Titan's surface, with radar footprints. Top panels contain, in order, crossovers A, B (**i**), C (**ii**), and D (**iii**); bottom panels contain crossovers E, F (**iv**), G, H (**v**), I, J, and K (**vi**).

Table 2. Summary of crossover identified. For each, the first row of the spacecraft altitude and incidence angle refers to the first flyby of the pair, the second row to the second flyby. The difference in mean anomaly ΔM has been computed, accounting for the effective difference in absolute tidal signal (the sign would only depend on the order of the flyby pair).

#	Flyby Pair	Lat. and Long.	Spacecraft Altitude	Incidence Angle	ΔM	ΔTidal Signal for h_2 = 2.5
A	T29 + T43	34.8°N, 144.1°W	14,643 km	0.43°	1°	0 m
			6955 km	0.31°		
B	T30 + T43	34.9°N, 145.7°W	7930 km	0.03°	1°	0 m
			6448 km	0.23°		
C	T41 + T64	9.4°N, 154.3°W	5853 km	0.05°	78°	15 m
			8197 km	0.21°		
D	Ta + T84	24.7°N, 3.4°E	7654 km	0.89°	12°	2 m
			5878 km	0.12°		
E	T28 + T29	12–20°S, 27–29°E	7626 km	0.46°	0°	0 m
			13,315 km	0.88°		
F	T29 + T30	5–12°S, 26–28°E	7408 km	0.39°	0°	0 m
			12,843 km	0.62°		
G	T19 + T55	38–39°N, 138–139°E	8592 km	0.33°	2°	0 m
			7063 km	0.46°		
H	T19 + T56	32.8°N, 140.8°E	14,873 km	0.28°	2°	0 m
			8043 km	0.12°		
I	T08 + T13	0°N, 172–180°E	6253 km	0.15°	79°	27 m
			10,580 km	0.03°		
J	T08 + T61	0°N, 172.7°E	8958 km	0.15°	94°	29 m
			5126 km	0.48°		
K	T13 + T61	0.3°N, 171.7°E	7106 km	0.03°	15°	3 m
			5416 km	0.52°		

There are a few more tracks that are close to overlap one with the other but that are not included in the list:

- T28 and T29 (outbound);
- T29 and T30 (outbound);
- T08 and T19;
- T77 and T113.

In these cases, the footprints do not overlap, or the intersection area is very small compared with the footprint's area, thus the probed region is different.

Note that altimetry data acquired during Ta, the first Titan flyby of the Cassini mission, might be affected by systematic error (mainly due to pointing inaccuracies) due to the poor knowledge of Titan ephemeris at the time of operation. Still, we decided to use its crossover with the T84 ground track (crossover D) since results show altimetry discrepancy at the crossover point consistent with other observations.

5. Trajectory Reconstruction of Cassini

To quantify the uncertainty associated with a crossover point associated with the orbital reconstruction, we reanalyzed the range and Doppler radiometric data collected from NASA's Deep Space Network (DSN) ground antennas during the selected flybys in order to reconstruct Cassini's trajectories around Titan. Note that altimetric data have not been used to update Cassini's orbits. We used JPL software MONTE (version 1.64, [34]) to analyze such data, following the classical orbit determination procedure performed by the Cassini NAV team (e.g., [35]). We followed the usual approach of reconstructing

a REV (a chunk of Cassini's orbit around Saturn, from "revolution"), with two flybys at most, which proved to be an optimal solution for reconstructing Cassini flybys with high accuracy and confidence. We tested whether reconstructing longer arcs (i.e., including three flybys) provided better accuracy, but we confirmed that orbital maneuvers between flybys essentially destroyed the coherence of the orbit to the level that a classical REV approach would be preferred due to its lower complexity and negligible increase in state uncertainty. For a given flyby, there are two possible orbital reconstructions (REVs) which can be used (i.e., T28 + T29 or T29 + T30, for T29). We selected, for each flyby, the REV that provided better accuracy for the flyby we were interested in. The same approach has also been followed by [36] for the analysis of Cassini range data in the context of planetary ephemeris generation.

In the Cassini dynamical model, we accounted for the gravitational acceleration coming from Saturnian main satellites and solar system planets (respectively, from satellite ephemerides sat389xl and planetary ephemeris de440, see NASA/NAIF website) in a relativistic 1-PN context, Titan's gravity field expansion up to degree and order 5 [22], and Saturn's zonal gravity field harmonic expansion up to degree 12 [37]. We did not account for Saturn's normal modes [37,38] due to the negligible effect they would have at Titan's distance. Since we used the latest available satellite ephemeris, Titan's state was not updated (contrary to the NAV team approach, e.g., [39]). Concerning the non-gravitational accelerations, we accounted for the solar radiation pressure acting on the Cassini spacecraft, the drag caused by Titan's atmosphere, and the anisotropic acceleration caused by the onboard RTGs. Additionally, we accounted for main engine and RCS thrust events, and for repointing maneuvers performed with the thruster.

To estimate the trajectory, we used a least-square estimation filter to adjust model parameters. For each arc, we estimated the Cassini state at the beginning of the observation arc, a drag and SRP coefficients, the three components of the RTG accelerations, large thrust firing and small burns, and empirical accelerations with constrained amplitude (following the procedure of the Cassini NAV team, e.g., [35]). In addition to our reconstruction of Cassini's flyby, we obtained the covariance matrix of model parameters, which allowed us to determine the evolution of position uncertainty over the flyby of our interest (see Figure 4). For a crossover, the largest contribution came from the radial component of the trajectory (for small off-nadir look angles).

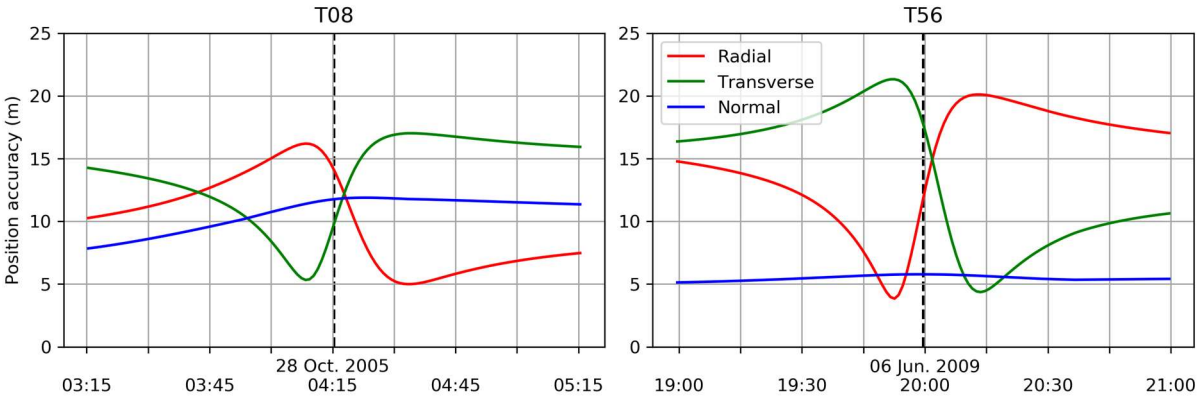

Figure 4. Uncertainty evolution (1-σ) of radial, transverse, and normal components of Cassini's position with respect to Titan, in selected passes (**left panel**: T08; **right panel**: T56). The vertical black line marks the epoch of the pericenter passage.

Correction to Crossover Points

The new orbits were used to update the ephemerides of Cassini and the relative altimetry tracks and thus the crossover points. The reconstructed spacecraft positions with respect to Titan can be compared with the one used to generate the altimetry data (contained in the SBDR data file). In the altimetry estimators, the spacecraft position x_{sc} at

each altimetry burst was updated to obtain the position at the center of the two-way light time window (after transmission of the burst at time t_i and reception after a Δt) with the velocity v_{sc}:

$$\widetilde{x}_{sc}(t_{active}) = x_{sc}(t_i) + v_{sc}(t_i) \cdot \delta t_{active}$$

where δt_{active} is the *active geometry time offset*, the delay after which the reception window is opened onboard the spacecraft, which is approximately equal to half the reception delay Δt.

The orbital corrections to each track of a crossover are reported in Table 3 for all the crossover points.

Table 3. Orbital correction and error budget for the crossover points. The sign of the orbital correction follows the altimetry: a positive correction means that the altimetry is larger, i.e., a smaller Cassini-surface distance. Each pass has a contribution from the orbital uncertainty and from the altimetry scatter (the column reports that of the corrected threshold estimator only). The error associated to a crossover is given by the RSS of the four different contributions. * Orbital uncertainty set to an average value, not computed for given pass.

#	Flyby Pair	Orbital Correction	Orbital Uncertainty	Altimetry Scatter	RSS
A	T29 + T43	39.6 m	39.4 m	26.4 m	60.1 m
		−24.5 m	25.8 m	26.3 m	
B	T30 + T43	53.1 m	25.7 m	22.6 m	50.1 m
		−24.5 m	25.5 m	26.3 m	
C	T41 + T64	5.3 m	13.1 m	15.5 m	26.2 m
		11.9 m	4.9 m	15.9 m	
D	Ta + T84	–	40.0 m *	9.4 m	61.1 m
		–	40.0 m *	21.2 m	
E	T28 + T29	30.2 m	12.3 m	17.5 m	41.6 m
		0.5 m	20.3 m	29.3 m	
F	T29 + T30	7.3 m	16.4 m	29.3 m	42.5 m
		−7.9 m	13.0 m	22.6 m	
G	T19 + T55	45.7 m	11.2 m	19.0 m	29.9 m
		14.5 m	13.6 m	15.0 m	
H	T19 + T56	48.8 m	10.9 m	19.0 m	36.8 m
		63.8 m	12.0 m	27.0 m	
I	T08 + T13	64.6 m	13.7 m	10.4 m	24.2 m
		−11.4 m	5.7 m	16.0 m	
J	T08 + T61	64.2 m	12.5 m	10.4 m	22.3 m
		21.6 m	5.6 m	14.2 m	
K	T13 + T61	−9.6 m	4.7 m	16.0 m	22.6 m
		21.1 m	5.4 m	14.2 m	

6. Crossover Error Budget

The difference in the recovered altimetry measured at the crossover can be related to:

- Errors in the reconstruction of Cassini's ephemerides with respect to Titan (radial direction);
- Instrumental errors of the altimeter (e.g., pointing angle);
- Errors in the processing of the collected waveforms;
- Physical displacement of Titan's surface due to tides.

The contribution from the accuracy of Cassini's orbits can be easily estimated from the covariance matrix of the passes we processed (see previous Section). We accounted only for the accuracy of the reconstructed ephemerides in the radial direction, as uncertainties in the non-radial directions were on the order of a few tens of meters, to be compared with the footprint size, which was of the order of tens of kilometers. Consequently, non-radial orbital uncertainties had a very limited effect on the footprint position and consequently on the reconstructed altimetric profile.

Residual errors from the waveform modeling of off-nadir contribution can also affect the measurement of interest and were challenging to quantify. An estimate of the random contribution from the altimeter can be obtained by measuring the scatter of the altimetry data. Since adjacent footprints had a large area overlap, the observed topography was highly correlated, thus the scatter from one point to the next was mostly representative of noise and should not be associated with an actual variation in topography. Therefore, for each estimator, a smoothing profile with the Savitzky–Golay algorithm was computed to retain the altimetric profile (see Section 3) and then compared with the altimetry value in order to single out the high-frequency scatter, whose standard deviation was associated with the accuracy of the altimetry measurements, per track. See Figure 5 for an example with the T13 pass, in the case of a corrected threshold estimator.

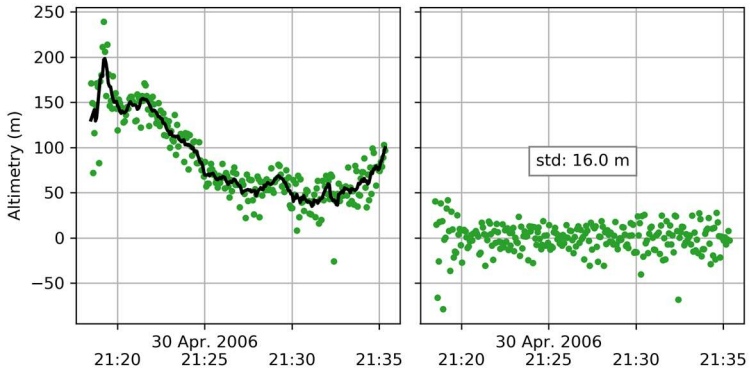

Figure 5. Left panel: altimetry from corrected threshold estimator for T13 and its smoothing; **right panel**: altimetry scatter, computed as the difference between altimetry and the smoothing curve.

The summary of the two contributions for each crossover is given in Table 3. Assuming that the altimetry scatter does not depend on the accuracy on the orbit, we can compute the squared sum of these four contributions to have an estimate of the variance of the crossover point δr_{ij} (composed by the i-th and j-th passes):

$$\sigma_{ij}^2 = \sigma_{orb,\,i}^2 + \sigma_{orb,\,j}^2 + \sigma_{alt,\,i}^2 + \sigma_{alt,\,j}^2$$

Note that, for a given pass, the orbital accuracy and altimetry accuracy can change from crossover to crossover, depending, respectively, on the actual time of observation and altimetry track during a pass. Results given in Table 3 show accuracies on the crossover points ranging from 22 to 60 m.

7. Results

The results of the analysis are reported in Figure 6, not accounting (top panels) or accounting (bottom panels) for the correction from our new reprocessed orbits, for the different altimetry estimators. Each crossover point has an uncertainty associated, given by the error budget previously presented (see Section 6). We can define both the root-

mean-square (RMS) and the weighted RMS (WRMS) of the crossover points δr_{ij} for a given estimator:

$$RMS = \sqrt{\frac{1}{N}\sum \delta r_{ij}^2} \quad WRMS = \sqrt{\frac{1}{N}\sum \left(\frac{\delta r_{ij}}{\sigma_{ij}}\right)^2}$$

They both give us indications about the quality of the altimetry measurements. The altimetry estimator with the smaller RMS indicates the best processing algorithm for altimetry data (assuming negligible contribution from the orbits and tides). Note that the WRMS should approach unity if (1) the crossovers are zero-mean randomly distributed and (2) the uncertainties are correctly associated. The results indicate that the smallest RMS is achieved with the corrected threshold and corrected first moment estimators, followed by the MLE and uncorrected threshold estimators. However, the uncorrected first moment estimator has the largest RMS, thus is expected to have the worst performance.

By looking at results without and with our orbital correction from Figure 6 it is possible to notice that the RMS of all estimators decreases when using the updated orbits. Except for the uncorrected first moment estimator, for which the improvement is limited, the decrease in the RMS of crossover points ranges from 8 to 15%. This clearly indicates that the updated orbits have higher quality since the discrepancy at crossover points decreases no matter the estimator used for the altimetry. This gives us confidence that the results shown in the bottom panels of Figure 6 are largely indicative of the accuracy of the altimetry processing.

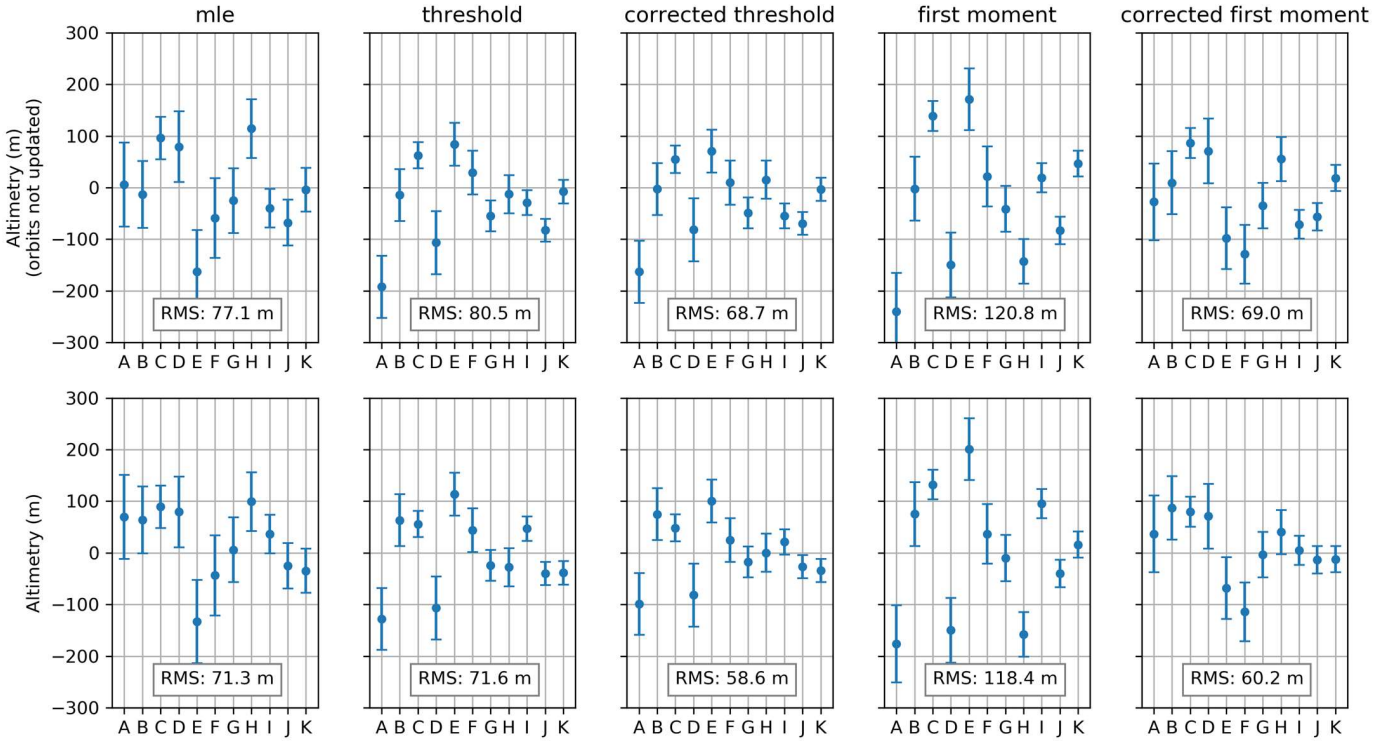

Figure 6. Crossover values for the different estimators. **Top panels** use orbits delivered to the radar team by Cassini NAV team, while **bottom panels** use updated orbits from our new orbital solutions. Solid tides are not accounted for.

7.1. Looking for Solid Tides

As anticipated, the solid tides can change the picture and provide an additional contribution to the crossover values. However, such a contribution is expected to be smaller than the intrinsic scatter we see in the crossover points, thus the tidal displacement signal is likely not recoverable from this dataset. If we assume a fully elastic response for Titan's

surface (i.e., h_2 = 2.5, see Section 2), the expected maximum tidal signal would be 22 m, corresponding to a maximum of 44 m peak-to-peak in a crossover with optimal observation conditions to be compared with crossover uncertainties ranging from 22 to 60 m (see Section 6). Although we cannot expect an accurate determination for the Love number h_2, from the crossover dataset, it is possible to provide an estimate via a least-square estimation filter, where each crossover is weighted based on error budget considerations. The RMS and WRMS of the different dataset, along with the estimated Love number, are reported in Table 4, in the case orbital corrections are accounted for (that is, related to the bottom panels of Figure 6). The RMS and WRMS only marginally decrease after fitting for the Love number h_2, indicating that the tidal signal is much smaller than the crossover errors. Note that, since the WRMS is larger than 1 for all the estimators (i.e., the uncertainties are likely underestimated or the crossover values still contain unmodeled effects), the 1-σ formal uncertainty of h_2 obtained from the least-square fit has been multiplied by the WRMS of the dataset in order to provide a more realistic evaluation of the uncertainty associated with the Love number.

Table 4. RMS and WRMS values for the different estimators, with the orbits updated from our new orbital solutions. *Crossovers with tides* refer to C, D, I, J, and K, whereas all the others are grouped in *crossover without tides*. The values in parenthesis refer to the crossover points obtained after fitting for h_2. Last row of the table reports estimates of the Love number h_2 for the different altimetry estimators, in the case the orbits are updated. Note that the fit for the Love number only marginally improves the RMS and WRMS of crossover values.

		MLE	**Threshold**	**Corrected Threshold**	**First Moment**	**Corrected First Moment**
RMS	All crossovers	71.3 m	71.6 m	58.6 m	118.4 m	60.2 m
	(after fit)	(70.3 m)	(71.5 m)	(58.6 m)	(116.2 m)	(59.8 m)
	Crossovers w/o tide	80.1 m	78.2 m	66.4 m	131.2m	68.5 m
	Crossovers w/ tide	59.0 m	62.9 m	47.5 m	100.9 m	48.4 m
	(after fit)	(56.4 m)	(62.6 m)	(47.5 m)	(95.3 m)	(47.2 m)
WRMS	All crossovers	1.20	1.75	1.39	2.57	1.27
	(after fit)	(1.16)	(1.75)	(1.39)	(2.45)	(1.26)
	Crossovers w/o tide	1.14	1.63	1.38	2.31	1.19
	Crossovers w/ tide	1.27	1.89	1.39	2.85	1.37
	(after fit)	(1.17)	(1.87)	(1.39)	(2.61)	(1.34)
	Love number h_2	2.5 ± 2.8	0.7 ± 2.6	0.2 ± 1.9	4.1 ± 4.2	1.1 ± 2.1

As expected, the uncertainty for the Love number h_2 is large and comparable to its estimated values, thus inconclusive for drawing new conclusions on Titan's interior. Note that only a few crossovers contribute to the determination of the Love number (i.e., mostly crossovers C, I, and J, see Table 2).

7.2. Influence of Observation Geometry

With the crossovers, we also identify the dependance upon key parameters of the radar observations, to understand whether the data have possible uncalibrated effects. The crossover values for the different estimators (the orbits are updated) as a function of the difference in the range from the surface at the time of the two observations are reported in the top panels of Figure 7. The idea is that observations of the same region of the moon made at different altitudes may provide different values due to instrumental effect. However, the results do not show a clear dependance of the crossover values with the difference in range for all the estimators.

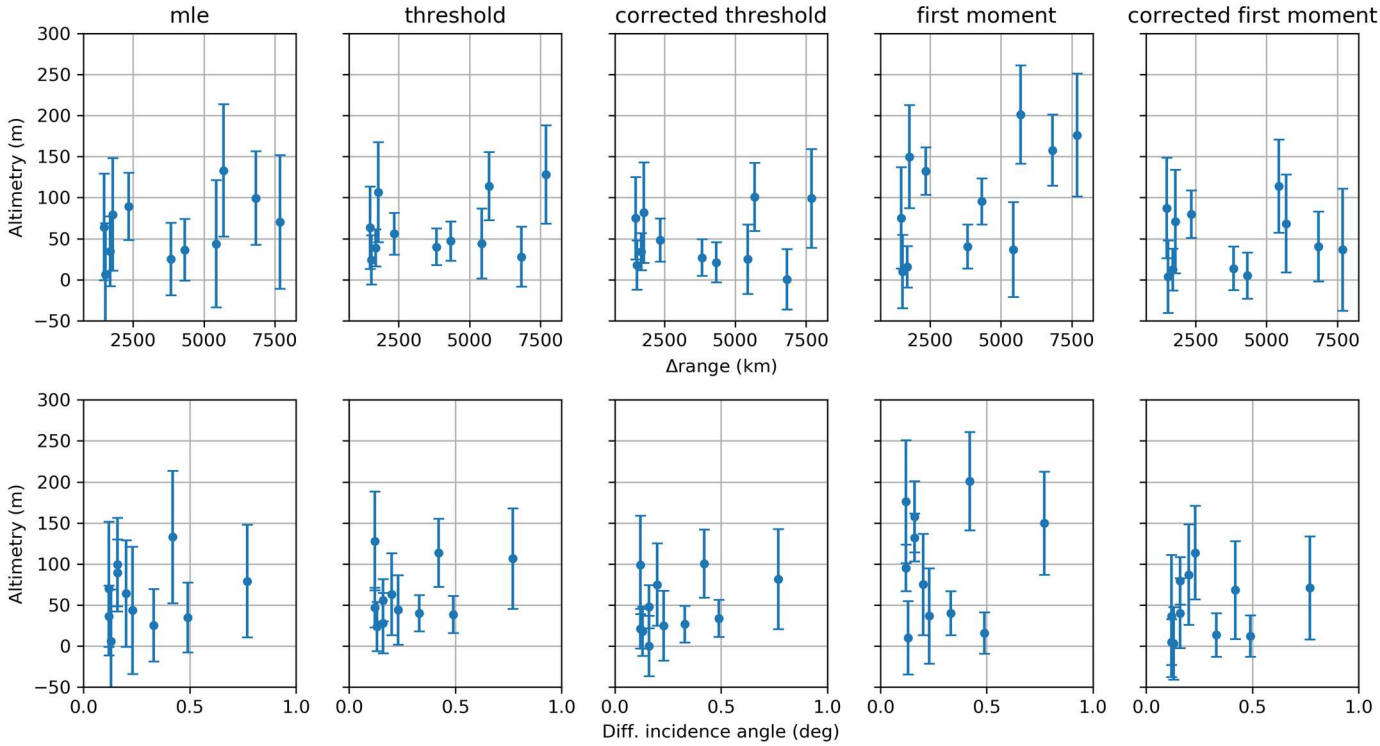

Figure 7. Crossover values for the different estimators, with the orbits updated from our new orbital solutions, as a function of the difference in the range from the surface at the time of the two observations (**top panels**) and as a function of the difference in the maximum incidence angle between the two observations (**bottom panels**).

The bottom panels of Figure 7 report the crossover values for the different estimators (with updated orbits) as a function of the difference in the incidence angle between the two observations. The results show that there is no evident correlation between the crossover values and this quantity, meaning that instrumental effects should be negligible.

8. Conclusions

In this work, we analyzed Cassini altimetric measurements and examined differences at altimetric crossovers. The altimetry measured at the crossover points shall be the same, if not for orbital errors, altimetry accuracy, and solid tides, which have never been measured on Titan. In order to reduce the contribution from orbital errors, new orbital solutions have been produced for the associated Cassini flybys by reanalyzing the navigation Doppler data. The results show that these new orbital solutions reduce the RMS of altimetry difference at crossover points, thus improving the associated systematic error. The analysis of altimetric data have shown that best altimetry performance can be associated with the corrected threshold and corrected first moment estimators, with an RMS value at crossover points of about 60 m for both the algorithms, compatible with error budget expectations.

Finally, the crossover values can hide the contribution coming from solid tides in the case the two passes flew over Titan when it was at different distances from Saturn, thus when the moon experienced a different tidal force. Fitting for the Love number h_2 (indicative of a surface displacement at orbital frequency) did not considerably improve the RMS at crossover points, indicating little to no contribution. The estimated values for the Love number h_2 had large uncertainty, which did not allow us to further constrain Titan's interior.

Future works incorporating delay-Doppler processing could potentially enhance our results by increasing the number of data points and improving the along-track resolution of the altimetric profiles. However, although the accuracy of radar measurements could

potentially increase, the error related to the spacecraft ephemerides position would not change, thus we do not expect a large improvement on the crossover points.

Author Contributions: Conceptualization, D.D., M.M., E.C. and L.I.; Methodology, D.D., M.M. and V.P.; Formal analysis, D.D., A.D.R. and V.N.; Data curation, M.M. and V.P.; Supervision, M.M. and L.I. All authors have read and agreed to the published version of the manuscript.

Funding: This work was supported in part by the Italian Space Agency.

Data Availability Statement: The altimeter data from the Cassini radar instrument are available through NASA's Planetary Data System (PDS), at the Cartography and Imaging Sciences Node (https://pds-imaging.jpl.nasa.gov, accessed on 10 June 2024). The raw tracking data and calibration files used for the reconstruction of Cassini orbits are available through NASA's PDS, at the Planetary Atmospheres Node (https://atmos.nmsu.edu, accessed on 10 June 2024). The geometry of the Cassini orbits, including SPK trajectory files and CK spacecraft attitude files, and Saturn satellite ephemeris, are available through NASA's Navigation and Ancillary Information Facility (NAIF, https://naif.jpl.nasa.gov, accessed on 10 June 2024). The MONTE navigation code (version 1.64) was obtained through a license agreement between NASA and the Italian Space Agency; the terms do not permit redistribution.

Conflicts of Interest: Authors A. Di Ruscio and V. Notaro were employed by the company Thales Alenia Space. The remaining authors declare that the research was conducted in the absence of any commercial or financial relationships that could be construed as a potential conflict of interest.

References

1. Elachi, C.; Wall, S.; Allison, M.; Anderson, Y.; Boehmer, R.; Callahan, P.; Encrenaz, P.; Flamini, E.; Franceschetti, G.; Gim, Y.; et al. Cassini radar views the surface of Titan. *Science* **2005**, *308*, 970–974. [CrossRef] [PubMed]
2. Lopes, R.M.C.; Malaska, M.J.; Schoenfeld, A.M.; Solomonidou, A.; Birch, S.P.D.; Florence, M.; Hayes, A.G.; Williams, D.A.; Radebaugh, J.; Verlander, T.; et al. A global geomorphologic map of Saturn's moon Titan. *Nat. Astron.* **2020**, *4*, 228–233. [CrossRef] [PubMed]
3. Lorenz, R.D.; Wall, S.; Radebaugh, J.; Boubin, G.; Reffet, E.; Janssen, M.; Stofan, E.; Lopes, R.; Kirk, R.; Elachi, C.; et al. The sand seas of Titan: Cassini RADAR observations of longitudinal dunes. *Science* **2006**, *312*, 724–727. [CrossRef] [PubMed]
4. Radebaugh, J. Dunes on Saturn's moon Titan as revealed by the Cassini Mission. *Aeolian Res.* **2013**, *11*, 23–41. [CrossRef]
5. Callegari, M.; Casarano, D.; Mastrogiuseppe, M.; Poggiali, V.; Notarnicola, C. Dune Height Estimation on Titan Exploiting Pairs of Synthetic Aperture Radar Images with Different Observation Angles. *IEEE J. Sel. Top. Appl. Earth Obs. Remote Sens.* **2015**, *8*, 1295–1306. [CrossRef]
6. Lalich, D.E.; Hayes, V.P.A.G.; Mastrogiuseppe, M.; Malaska, M.J.; Schurmeier, L.R. Diverse evolution of mountains and hummocks on Titan as observed by the Cassini RADAR altimeter. *Icarus* **2022**, *374*, 114775. [CrossRef]
7. Hayes, A.G. The lakes and seas of Titan. *Annu. Rev. Earth Planet. Sci.* **2016**, *44*, 57–83. [CrossRef]
8. Hayes, A.G.; Birch, S.P.D.; Dietrich, W.E.; Howard, A.D.; Kirk, R.L.; Poggiali, V.; Mastrogiuseppe, M.; Michaelides, R.J.; Corlies, P.M.; Moore, J.M.; et al. Topographic constraints on the evolution and connectivity of Titan's lacustrine basins. *Geophys. Res. Lett.* **2017**, *44*, 11745–11753. [CrossRef]
9. Michaelides, R.J.; Hayes, A.G.; Mastrogiuseppe, M.; Zebker, H.A.; Farr, T.G.; Malaska, M.J.; Poggiali, V.; Mullen, J. Constraining the physical properties of Titan's empty lake basins using nadir and off-nadir Cassini RADAR backscatter. *Icarus* **2016**, *270*, 57–66. [CrossRef]
10. Mitri, G.; Barnes, J.; Coustenis, A.; Flamini, E.; Hayes, A.; Lorenz, R.D.; Mastrogiuseppe, M.; Orosei, R.; Postberg, F.; Reh, K.; et al. Exploration of Enceladus and Titan: Investigating ocean worlds' evolution and habitability in the Saturn system. *Exp. Astron.* **2021**, *54*, 877–910. [CrossRef]
11. Mastrogiuseppe, M.; Poggiali, V.; Hayes, A.G.; Lorenz, R.; Lunine, J.I.; Picardi, G.; Seu, R.; Flamini, E.; Mitri, G.; Notarnicola, C.; et al. The bathymetry of a Titan sea. *Geophys. Res. Lett.* **2014**, *41*, 1432–1437. [CrossRef]
12. Hayes, A.G.; Lorenz, R.D.; Lunine, J.I. A post-Cassini view of Titan's methane-based hydrologic cycle. *Nat. Geosci.* **2018**, *11*, 306–313. [CrossRef]
13. Poggiali, V.; Mastrogiuseppe, M.; Hayes, A.G.; Seu, R.; Birch, S.P.D.; Lorenz, R.; Grima, C.; Hofgartner, J.D. Liquid-filled canyons on Titan. *Geophys. Res. Lett.* **2016**, *43*, 7887–7894. [CrossRef]
14. Birch, S.P.D.; Hayes, A.G.; Dietrich, W.E.; Howard, A.D.; Bristow, C.S.; Malaska, M.J.; Moore, J.; Mastrogiuseppe, M.; Hofgartner, J.; Williams, D.; et al. Geomorphologic mapping of titan's polar terrains: Constraining surface processes and landscape evolution. *Icarus* **2017**, *282*, 214–236. [CrossRef]
15. Mastrogiuseppe, M.; Hayes, A.G.; Poggiali, V.; Seu, R.; Lunine, J.I.; Hofgartner, J.D. Radar Sounding Using the Cassini Altimeter: Waveform Modeling and Monte Carlo Approach for Data Inversion of Observations of Titan's Seas. *IEEE Trans. Geosci. Remote Sens.* **2016**, *54*, 5646–5656. [CrossRef]

16. Mastrogiuseppe, M.; Hayes, A.G.; Poggiali, V.; Lunine, J.I.; Lorenz, R.D.; Seu, R.; Le Gall, A.; Notarnicola, C.; Mitchell, K.; Malaska, M.; et al. Bathymetry and composition of Titan's Ontario Lacus derived from Monte Carlo-based waveform inversion of Cassini RADAR altimetry data. *Icarus* **2018**, *300*, 203–209. [CrossRef]
17. Mastrogiuseppe, M.; Poggiali, V.; Hayes, A.G.; Lunine, J.I.; Seu, R.; Di Achille, G.; Lorenz, R. Cassini radar observation of Punga Mare and environs: Bathymetry and composition. *Earth Planet. Sci. Lett.* **2018**, *496*, 89–95. [CrossRef]
18. Mastrogiuseppe, M.; Poggiali, V.; Hayes, A.G.; Lunine, J.I.; Seu, R.; Mitri, G.; Lorenz, R.D. Deep and methane-rich lakes on Titan. *Nat. Astron.* **2019**, *3*, 535–542. [CrossRef]
19. Poggiali, V.; Hayes, A.G.; Mastrogiuseppe, M.; Le Gall, A.; Lalich, D.; Gomez-Leal, I.; Lunine, J.I. The Bathymetry of Moray Sinus at Titan's Kraken Mare. *J. Geophys. Res. Planets* **2020**, *125*, e2020JE006558. [CrossRef]
20. Le Gall, A.; Malaska, M.J.; Lorenz, R.D.; Janssen, M.A.; Tokano, T.; Hayes, A.G.; Mastrogiuseppe, M.; Lunine, J.I.; Veyssière, G.; Encrenaz, P.; et al. Composition, seasonal change, and bathymetry of Ligeia Mare, Titan, derived from its microwave thermal emission. *J. Geophys. Res. Planets* **2016**, *121*, 233–251. [CrossRef]
21. Iess, L.; Jacobson, R.A.; Ducci, M.; Stevenson, D.J.; Lunine, J.I.; Armstrong, J.W.; Asmar, S.W.; Racioppa, P.; Rappaport, N.J.; Tortora, P. The Tides of Titan. *Science* **2012**, *337*, 457–459. [CrossRef] [PubMed]
22. Durante, D.; Hemingway, D.J.; Racioppa, P.; Iess, L.; Stevenson, D.J. Titan's gravity field and interior structure after Cassini. *Icarus* **2019**, *326*, 123–132. [CrossRef]
23. Zebker, H.A.; Stiles, B.; Hensley, S.; Lorenz, R.; Kirk, R.L.; Lunine, J. Size and shape of Saturn's moon Titan. *Science* **2009**, *324*, 921–923. [CrossRef] [PubMed]
24. Corlies, P.; Hayes, A.G.; Birch, S.P.D.; Lorenz, R.; Stiles, B.W.; Kirk, R.; Poggiali, V.; Zebker, H.; Iess, L. Titan's Topography and Shape at the End of the Cassini Mission. *Geophys. Res. Lett.* **2017**, *44*, 11754–11761. [CrossRef]
25. Vincent, D.; Karatekin, Ö.; Vallaeys, V.; Hayes, A.G.; Mastrogiuseppe, M.; Notarnicola, C.; Dehant, V.; Deleersnijder, E. Numerical study of tides in Ontario Lacus, a hydrocarbon lake on the surface of the Saturnian moon Titan. *Ocean Dyn.* **2016**, *66*, 461–482. [CrossRef]
26. Mastrogiuseppe, M. Dual Frequency Orbiter-Radar System for the Observation of Seas and Tides on Titan: Extraterrestrial Oceanography from Satellite. *Remote Sens.* **2019**, *11*, 1898. [CrossRef]
27. Elachi, C.; Allison, M.D.; Borgarelli, L.; Encrenaz, P.; Im, E.; Janssen, M.A.; Johnson, W.T.K.; Kirk, R.L.; Lorenz, R.D.; Lunine, J.I.; et al. Radar: The Cassini Titan Radar Mapper. In *The Cassini-Huygens Mission*; Russell, C.T., Ed.; Springer: Dordrecht, The Netherlands, 2004. [CrossRef]
28. West, R.D.; Anderson, Y.; Boehmer, R.; Borgarelli, L.; Callahan, P.; Elachi, C.; Gim, Y.; Hamilton, G.; Hensley, S.; Janssen, M.A.; et al. Cassini RADAR sequence planning and instrument performance. *IEEE Trans. Geosci. Remote Sens.* **2009**, *47*, 1777–1795. [CrossRef]
29. Montefredini, E.; Morelli, F.; Picardi, G.; Seu, R. A non-coherent surface backscattering model for radar observation of planetary bodies and its application to Cassini Radar Altimeter. *Planet. Space Sci.* **1995**, *43*, 1567–1577. [CrossRef]
30. Alberti, G.; Festa, L.; Papa, C.; Vingione, G. A Waveform Model for Near-Nadir Radar Altimetry Applied to the Cassini Mission to Titan. *IEEE Trans. Geosci. Remote Sens.* **2009**, *47*, 7. [CrossRef]
31. Bucciarelli, T.; Cacopardi, S.; Picardi, G.; Seu, R.; Levrini, G.; Perfetti, R. Tracking Algorithms in Radar Altimetry. In Proceedings of the International Geoscience and Remote Sensing Symposium (IGARSS'88), Edinburgh, UK, 13–16 September 1988; Volume 2, pp. 973–976.
32. Poggiali, V.; Mastrogiuseppe, M.; Hayes, A.G.; Seu, R.; Mullen, J.P.; Birch, S.P.D.; Raguso, M.C. High resolution topography of Titan adapting the Delay-Doppler algorithm to the Cassini RADAR Altimeter Data. *IEEE Trans. Geosci. Remote Sens.* **2019**, *57*, 7262–7268. [CrossRef]
33. Mastrogiuseppe, M.; Poggiali, V.; Seu, R.; Martufi, R.; Notarnicola, C. Titan dune heights retrieval by using Cassini Radar Altimeter. *Icarus* **2014**, *230*, 191–197. [CrossRef]
34. Evans, S.; Taber, W.; Drain, T.; Smith, J.; Wu, H.; Guevara, M.; Sunseri, R.; Evans, J. MONTE: The next generation of mission design and navigation software. In Proceedings of the 6th International Conference on Astrodynamics Tools and Techniques, Darmstadt, Germany, 14–17 March 2016.
35. Bellerose, J.; Roth, D.; Wagner, S. The Cassini Mission: Reconstructing Thirteen Years of the Most Complex Gravity-Assist Trajectory Flown to Date. In Proceedings of the 2018 SpaceOps Conference, Marseille, France, 28 May–1 June 2018. [CrossRef]
36. Di Ruscio, A.; Fienga, A.; Durante, D.; Iess, L.; Laskar, J.; Gastineau, M. Analysis of Cassini radio tracking data for the construction of INPOP19a: A new estimate of the Kuiper belt mass. *Astron. Astrophys.* **2020**, *640*, A7. [CrossRef]
37. Iess, L.; Militzer, B.; Kaspi, Y.; Nicholson, P.; Durante, D.; Racioppa, P.; Anabtawi, A.; Galanti, E.; Hubbard, W.; Mariani, M.J.; et al. Measurement and implications of Saturn's gravity field and ring mass. *Science* **2019**, *364*, aat2965. [CrossRef] [PubMed]
38. Markham, S.; Durante, D.; Iess, L.; Stevenson, D.J. Possible evidence of p-modes in Cassini measurements of Saturn's gravity field. *Planet. Sci. J.* **2020**, *1*, 27. [CrossRef]
39. Boone, D.; Bellerose, J.; Roth, D. Resolution of Orbit Determination prediction instabilities at Titan during Cassini's Solstice mission. In Proceedings of the 26th International Symposium on Space Flight Dynamics, Matsuyama, Japan, 3–9 June 2017; p. ISSFD-2017-109.